

# Transient Analysis of an Induction Motor and its Control System using Cosimulation

V. M. Jimenez-Mondragon, I. Lopez-Garcia,  
R. Escarela-Perez and F. Gonzalez-Montañez  
*Departamento de energía*  
*Universidad Autónoma Metropolitana-Azcapotzalco*  
Azcapotzalco, México  
e-mail: vmjm@azc.uam.mx, ilg@azc.uam.mx,  
r.escarela@ieee.org, f.g.mx@ieee.org

H. Mujica-Ortega  
*Departamento de control y robótica*  
*División de ingeniería eléctrica, FI*  
*Universidad Nacional Autónoma de México*  
C.U., Coyoacán, México  
hmujica@unam.mx

**Abstract**—A virtual test bench based on the cosimulation of finite element analysis and circuit simulation has been applied to evaluate controllers in three-phase induction motors. A finite element model is used to carry out the electromagnetic analysis of the induction machine. This model has the advantage of considering a precise distribution of induced eddy-currents, the material nonlinearity, space and time harmonics, and torque pulsation. The speed and rotor magnetic flux norm tracking problems are tackled with a nonlinear passivity-based control. The results show the existence of an overexcitation problem in the control action when the motor operates at full load and nominal speed. This problem was not so evident in the state space simulation, which confirms that the use of this cosimulation platform represents a helpful and reliable starting point before experimentally implementing the controller.

## I. INTRODUCTION

Nowadays, electromagnetic devices have a wide variety of applications among which are hybrid vehicles, magnetic levitation systems, electric actuators, and wind turbines. The design, control, and optimization of these systems are complicated without the use of precise simulation tools. The use of field-circuit coupled models stands out among others because the results are similar to the real operating characteristics of the system since the electromagnetic phenomenon of the device is considered through the finite element (FE) model. It also reduces the number of experimental prototypes that are expensive in most cases [1].

A field-circuit coupled model simultaneously uses the magnetic field solver and circuit solver [2], [3], which provides an accurate virtual prototype to address the control problem of an induction motor modeled by finite elements. A simulation platform is useful if it accurately represents reality, and is easy to manipulate and implement. All these features are available in the platform used in this work. The cosimulation of FE analysis and circuit simulation has been used for decades to address the control problem in electrical machines. Remarkable works reported in the literature where cosimulation is used can be found at [4]–[9].

On the other hand, the induction machine speed control is of industrial interest due to the multiple processes in which it is embedded. Currently, there are different strategies that allow

the control of induction motors such as: PID control [10], field-oriented indirect control [11], passivity-based control (PBC) [12], [13], field-oriented direct control [14], etc. The passivity-based control reported in [12] is used in this work, because of the high dynamic performance that can be achieved with highly variable speed profiles.

The work is organized as follows. Section II presents the field-circuit formulation to solve the induction motor problem by Finite Element Method (FEM). The high-performance PBC for speed and rotor magnetic flux norm tracking is briefly treated in section III. Section IV explains the cosimulation of the FE analysis and control system. Finally, the results for a 10 HP induction motor are presented and analyzed in section V.

## II. FIELD-CIRCUIT COUPLED FORMULATION

In general, the low-frequency transient problem of the motor is described by the following discrete system of differential-algebraic equations:

$$[D] \{\dot{x}\} + [S] \{x\} + \{f\} = 0 \quad (1)$$

where  $\dot{x} = \frac{\partial x}{\partial t}$  and  $\{x\}$  is a state variables vector. The damping matrix  $[D]$  and stiffness matrix  $[S]$  can be dependent on the unknown  $x$  and time.  $\{f\}$  is an excitation vector where the control signals (stator voltages) are incorporated.

The discrete system of the form given in (1) for the cartesian field problem and field-circuit coupling equations for solid (squirrel cage bars) and filamentary (stator windings) conductors are presented in the next sections.

### A. Nonlinear diffusion equation

The manipulation of Maxwell's equations leads to the following nonlinear diffusion equation to solve the time-domain 2D-cartesian motor problem [15]:

$$\begin{aligned} \frac{\partial}{\partial x} \left( \nu \frac{\partial A_z}{\partial x} \right) + \frac{\partial}{\partial y} \left( \nu \frac{\partial A_z}{\partial y} \right) &= -J_{fz} - J_{sz} \\ &= -J_{fz} + \sigma \left( \frac{\partial A_z}{\partial t} - \frac{v_s}{l_{eff}} \right) \end{aligned} \quad (2)$$

where  $A_z$  is the only component of the magnetic vector potential.  $J_{fz}$ ,  $J_{sz}$  and  $v_s$  are the current density in regions with filamentary conductors, the current density in regions with solid conductors and the potential difference between the ends of the solid conductors, respectively.  $\sigma$  and  $l_{eff}$  are the conductivity and the axial length, respectively.  $\nu$  is the reluctivity of the material and can be a nonlinear function of the magnetic field.

Filamentary conductors are considered thin such that eddy-currents are negligible. This way, each domain  $\Omega_f$  with cross-section  $\Lambda_f$  has a uniform distribution of  $N_f$  series-connected filamentary conductors, which carry a current  $I_f$ . Then, the current density can be expressed as:

$$J_{fz} = \frac{N_f i_f}{\Lambda_f} \quad (3)$$

Substitution of (3) into (2) leads to the boundary-value problem for the cartesian magnetic field:

$$\frac{\partial}{\partial x} \left( \nu \frac{\partial A_z}{\partial x} \right) + \frac{\partial}{\partial y} \left( \nu \frac{\partial A_z}{\partial y} \right) = -\frac{N_f i_f}{\Lambda_f} + \sigma \left( \frac{\partial A_z}{\partial t} - \frac{v_s}{l_{eff}} \right) \quad (4)$$

Three domains of interest are considered in (4): non-conductor, solid and filamentary regions. Each one of these is found in an induction machine.

### B. Space discretization

The FE equations in the different domains are obtained by Galerkin's approximation [16]. This method is based on the minimization of an integral expression and is a special case of the weighted residual method. The integral expression is:

$$\int W_p R_e dS = 0 \quad (5)$$

where  $R_e$  is a residual, which is obtained by setting to zero the partial differential equation (4). Shape functions  $\zeta_i$  in the Galerkin's method are used to approximate the magnetic vector potential in an element with a polynomial function of the form:

$$A_z = \sum a_i(t) \zeta_i(x, y) \quad (6)$$

The equation (4) can be expressed numerically by the FEM as [17]:

$$-[S]\{a\} - \sum_s [D_s]\{\dot{a}\} + \sum_f [S_f]i_f + \sum_s [S_s]v_s = 0 \quad (7)$$

where  $\dot{a} = \partial a / \partial t$ . The matrices and vectors in (7) are defined as follows:

Stiffness matrix:

$$[S]_{n \times n} = \sum_e \iint_{\Omega_e} \nu \left( \frac{\partial \zeta}{\partial x} \frac{\partial \zeta^T}{\partial x} + \frac{\partial \zeta}{\partial y} \frac{\partial \zeta^T}{\partial y} \right) dx dy \quad (8)$$

Conductivity matrix:

$$[D_s]_{n \times n} = \sum_e \iint_{\Omega_e} \sigma \zeta \zeta^T dx dy \quad (9)$$

Winding vector in regions with filamentary conductors:

$$[S_f]_n = \frac{N_f}{\Lambda_f} \sum_{e_f} \iint_{\Omega_{e_f}} \zeta dx dy \quad (10)$$

Winding vector in regions with solid conductors:

$$[S_s]_n = \frac{\sigma}{l_{eff}} \sum_{e_s} \iint_{\Omega_{e_s}} \zeta dx dy \quad (11)$$

where  $n$  is the number of nodes in the FE mesh. The stiffness and conductivity matrices contain information about the geometry and physical properties of the motor. The solid and filamentary winding vectors allow the interconnection of the FE model with the external circuit and therefore with the control stage.

### C. Coupling equation: filamentary conductor

The unknowns in (7) to solve the field-circuit coupled problem in regions with filamentary conductors are the magnetic vector potential and the current  $i_f$  in each winding. The voltage-current relation for a winding is used as an additional circuit equation. This can be expressed in terms of the magnetic vector potential as:

$$v_f = r_f i_f + l_{eff} N_f \frac{\partial}{\partial t} \frac{\iint_{\Omega_f} A_z dx dy}{\Lambda_f} \quad (12)$$

where  $r_f$  is the dc winding resistance. This equation is fundamental because it allows the coupling of the field model with the external circuit and the control stage. The second term on the right side in (12) is the induced voltage in the filamentary winding. The FE discretization of the voltage-current relation (12) is given by:

$$v_f = r_f i_f + [D_f]^T \{\dot{a}\} \quad (13)$$

where:

$$[D_f]_n = \frac{l_{eff} N_f}{\Lambda_f} \sum_{e_f} \iint_{\Omega_f} \zeta dx dy \quad (14)$$

and it is obtained by using the polynomial approximation of the magnetic vector potential defined in (6). The discrete system in the general form defined in (1) for regions with filamentary conductors is obtained through the voltage-current relation (13) and the winding vector (10):

$$\underbrace{\begin{bmatrix} 0 & 0 & 0 & 0 \\ 0 & 0 & 0 & 0 \\ 0 & 0 & 0 & 0 \\ -D_f^T & 0 & 0 & 0 \end{bmatrix}}_D \begin{bmatrix} \dot{a} \\ \dot{v}_p \\ \dot{v}_q \\ \dot{i}_f \end{bmatrix} + \underbrace{\begin{bmatrix} 0 & 0 & 0 & S_f \\ 0 & 0 & 0 & 1 \\ 0 & 0 & 0 & -1 \\ 0 & 1 & -1 & -r_f \end{bmatrix}}_S \begin{bmatrix} a \\ v_p \\ v_q \\ i_f \end{bmatrix} = \underbrace{\begin{bmatrix} 0 \\ 0 \\ 0 \\ 0 \end{bmatrix}}_f \quad (15)$$

where  $v_f = v_p - v_q$ . The third term in (7) has been incorporated in (15) to obtain a coupling block between the field system with filamentary regions and the external circuit.

#### D. Coupling equation: solid conductor

The discrete system block for solid conductors is obtained in this section. In the field problem (4) with solid conductor regions the unknowns are the potential difference between the conductor terminals  $v_s$  and the magnetic vector potential. The total current in a solid conductor is defined as follows:

$$i_t = i_e + i_s \quad (16)$$

where  $i_e$  is the induced current and  $i_s$  is the source current. Expressing the total current in terms of the state variables leads to:

$$i_t = -\sigma \iint_{\Omega_s} \frac{\partial A_z}{\partial t} dx dy + \frac{\sigma}{l_{eff}} \iint_{\Omega_s} (v_p - v_q) dx dy \quad (17)$$

Substituting the polynomial approximation of the potential given by (6) in (17) leads to the FE version of (16):

$$i_t = [D_m]^T \{\dot{a}\} + G(v_p - v_q) \quad (18)$$

where:

$$[D_m]_n = \sum_{e_s} \iint_{\Omega_{e_s}} -\sigma \zeta dx dy \quad (19)$$

and  $G$  is the conductance defined as:

$$G = \frac{\sigma \Lambda_s}{l_{eff}} \quad (20)$$

$\Lambda_s$  is the cross section area of the region  $\Omega_s$ . From (18) and (11), the field-circuit coupling block for solid conductors in the general form defined by (1) is:

$$\underbrace{\begin{bmatrix} 0 & 0 & 0 \\ D_m^T & 0 & 0 \\ -D_m^T & 0 & 0 \end{bmatrix}}_D \begin{bmatrix} \dot{a} \\ \dot{v}_p \\ \dot{v}_q \end{bmatrix} + \underbrace{\begin{bmatrix} 0 & S_s & -S_s \\ 0 & G & -G \\ 0 & -G & G \end{bmatrix}}_S \begin{bmatrix} a \\ v_p \\ v_q \end{bmatrix} = \mathbf{0} \quad (21)$$

#### E. Complete finite-element discrete system

The discrete blocks for the electromagnetic field system (7), (15) and (21) are coupled through the magnetic vector potential, the current in filamentary regions and the potential difference at the ends of the solid conductors. The discrete block of the cartesian field problem can be expressed in matrix form as follows:

$$\underbrace{\begin{bmatrix} -D_s & 0 & 0 & 0 & 0 & 0 \\ 0 & 0 & 0 & 0 & 0 & 0 \\ 0 & 0 & 0 & 0 & 0 & 0 \\ D_m^T & 0 & 0 & 0 & 0 & 0 \\ -D_m^T & 0 & 0 & 0 & 0 & 0 \\ -D_f^T & 0 & 0 & 0 & 0 & 0 \end{bmatrix}}_D \begin{bmatrix} \dot{a} \\ \dot{v}_{pf} \\ \dot{v}_{qf} \\ \dot{v}_{ps} \\ \dot{v}_{qs} \\ \dot{i}_f \end{bmatrix} \quad (22)$$

$$+ \underbrace{\begin{bmatrix} -S & 0 & 0 & S_s & -S_s & S_f \\ 0 & 0 & 0 & 0 & 0 & 1 \\ 0 & 0 & 0 & 0 & 0 & -1 \\ 0 & 0 & 0 & G & -G & 0 \\ 0 & 0 & 0 & -G & G & 0 \\ 0 & 1 & -1 & 0 & 0 & -r_f \end{bmatrix}}_S \begin{bmatrix} a \\ v_{pf} \\ v_{qf} \\ v_{ps} \\ v_{qs} \\ i_f \end{bmatrix} = 0$$

where  $v_{pf}$  and  $v_{qf}$  are the nodal voltages between the ends of each winding  $f$ . These voltages allow the electromagnetic system to be interconnected with the external circuit through the control signals.  $v_{ps}$  and  $v_{qs}$  are the nodal voltages between the ends of each solid conductor  $s$ . The system (22) is asymmetric. However, symmetry is recovered once it is discretized in the time domain by the backward Euler method and linearized with the Newton-Raphson method [17].

### III. PASSIVITY-BASED CONTROL

Consider the nonlinear PBC for speed and rotor magnetic flux norm tracking reported in [12], specifically  $\lim_{t \rightarrow \infty} |\omega - \omega_d| = 0$  and  $\lim_{t \rightarrow \infty} \|\psi_r\| - \|\psi_{rd}\| = 0$ , where  $\omega_d$  is the desired speed and  $\|\psi_{rd}\|$  is the desired norm of rotor magnetic fluxes, under the following assumptions:

- S.1 Stator currents  $I_s$ , speed  $\omega$  and rotor acceleration  $\dot{\omega}$  are measured. These last two measurements will be estimated by the differentiation methods evaluated in [12].
- S.2 All model parameters are known.
- S.3 Load torque  $\tau_L(t)$  is an unknown function.
- S.4 The desired rotor speed  $\omega_d(t)$  is a bounded and twice differentiable function.
- S.5 The desired rotor magnetic flux norm  $\|\psi_{rd}\|$  is a strictly positive, smooth and bounded exogenous function.

Starting from the induction motor model  $ab$ , described in [13] as a set of five differential equations; the state error and its dynamics are defined as,

$$e = \begin{bmatrix} e_{I_s} \\ e_{\psi_r} \\ e_{\omega} \end{bmatrix} = x - x_d \implies \dot{e} = \begin{bmatrix} \dot{e}_{I_s} \\ \dot{e}_{\psi_r} \\ \dot{e}_{\omega} \end{bmatrix} = \dot{x} - \dot{x}_d \quad (23)$$

where the state vector  $x \triangleq [I_s^T, \psi_r^T, \omega]^T \in \mathbb{R}^5$ .

Therefore, the desired state vector is set as  $x_d \triangleq [I_{sd}^T, \psi_{rd}^T, \omega_d]^T$ . The structure of the control law applied to stator voltages is given by

$$U_s = \sigma \dot{I}_{sd} + \frac{n_p L_{sr}}{L_r} \mathcal{J} \omega_d \psi_{rd} + \left( \frac{L_{sr}^2 R_r}{L_r^2} + R_s \right) I_{sd} - \frac{L_{sr} R_r}{L_r^2} \psi_{rd} - K_{I_s} e_{I_s}, \quad (24)$$

where a constant damping term  $K_{I_s}$  is included in the current error  $e_{I_s}$ . The vector of desired stator currents is given by

$$I_{sd} = \frac{L_r}{R_r L_{sr}} \left( \dot{\psi}_{rd} - n_p \omega_d \mathcal{J} \psi_{rd} + \frac{R_r}{L_r} \psi_{rd} \right) \quad (25)$$

The desired time-varying rotor fluxes are obtained as a dynamic system solution

$$\dot{\psi}_{rd} = \left[ n_p \omega_d + \frac{R_r}{n_p \beta^2} \tau_d \right] \mathcal{J} \psi_{rd} + \frac{\dot{\beta}}{\beta} \psi_{rd}, \quad \psi_{rd}(0) = \begin{bmatrix} \beta \\ 0 \end{bmatrix} \quad (26)$$

while the desired electromagnetic torque  $\tau_d$  is defined as:

$$\tau_d = J \dot{\omega}_d + B \omega_d + \hat{\tau}_L - K_\omega e_\omega, \quad (27)$$

where

$$\hat{\tau}_L = -K_{\omega i} \int e_\omega dt, \quad K_{\omega i} > 0, \quad \hat{\tau}_L(0) = 0. \quad (28)$$

The derivative of  $I_{sd}$  required for the implementation of the control law (24) is obtained analytically and is given by

$$\begin{aligned} \dot{I}_{sd} = & \frac{L_r}{L_{sr} n_p} \left[ \left( \frac{\dot{\tau}_d - 2\tau_d \dot{\beta}}{\beta} \right) \mathcal{J} \psi_{rd} + \left( \frac{\tau_d}{\beta^2} \right) \mathcal{J} \dot{\psi}_{rd} \right] \\ & + \frac{L_r}{R_r L_{sr}} \left[ \left( \frac{\dot{\beta} \beta - \dot{\beta}^2}{\beta^2} \right) \psi_{rd} + \left( \frac{\dot{\beta}}{\beta} \right) \dot{\psi}_{rd} \right] + \frac{\dot{\psi}_{rd}}{L_{sr}}, \quad (29) \end{aligned}$$

as well as the derivative of  $\tau_d$  defined by

$$\dot{\tau}_d = J \ddot{\omega}_d + B \dot{\omega}_d + \dot{\hat{\tau}}_L - K_\omega \dot{e}_\omega. \quad (30)$$

#### IV. FIELD-CIRCUIT COUPLED MODEL

The field-circuit coupling problem can be solved by the strong coupling method or by the indirect method. The strong coupling method solves simultaneously the FE system defined by (22) and the external circuit equations with the control stage at each time step. This method finds solutions for greater precision and speed. However, specific codes have to be implemented to solve the control problem.

The field-circuit coupling problem has also been solved using the indirect method, where the field model (22) and the external circuit with the control stage defined in section III are solved as separate systems. In this case, the solution of each system is used to excite the other one in an iterative procedure. Therefore, each system is autonomously developed with its own mathematical and numerical methods. The main advantages of this method are flexibility and modularity because it allows the use of already tested circuit software.

This work is based on the cosimulation of the FE model and the circuit system. The cosimulation of the whole problem is performed in Matlab-Simulink environment. The stator currents and position are calculated from the FE model and these are the input variables at the controller. The control outputs are the stator voltages, which in turn are the input signals for the FE model. The implemented model in Matlab-Simulink is shown in Fig. 1.

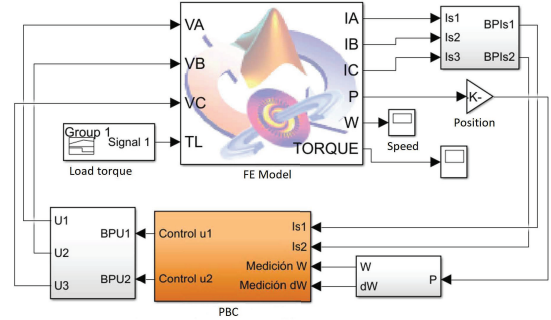


Fig. 1. Virtual test bench based on the cosimulation.

#### V. RESULTS AND DISCUSSION

Numerical tests were carried out for a model of a 10 HP, 2 poles, 50 Hz and 380 Vrms squirrel cage induction motor. The rotor has a double squirrel cage with 20 aluminum bars. The three-phase lap winding has 208 turns per phase. Fig. 2 shows the motor geometry, the FE meshing, and the boundary conditions. The FE model was implemented in the well known commercial software Altair Flux2D [18]. The mesh has 3464 second-order elements and 7235 nodes and it takes advantage of antiperiodic boundary conditions. The nonlinearity of the ferromagnetic material of the stator and the rotor cores is taken into account with the FE transient model.

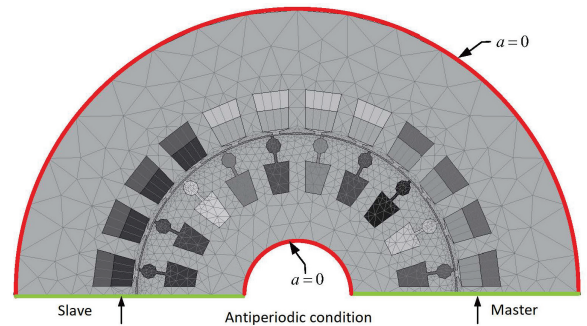


Fig. 2. Induction motor cross section [18].

Numerical tests involve the problem of speed and rotor magnetic flux norm tracking. The flux norm is kept constant at its nominal value of 1.7 Wb. The speed profile requires accelerating the machine from a rest condition to its nominal speed of 304 rad/s in 0.5 s and gradually decelerate until 44 rad/s from t=1 s. The motor starts at the no-load condition and between 0.7 s and 1.2 s the nominal load torque of 24.7 N-m

is applied. The tuning parameters for the PBC were considered as:  $K_\omega = 5$ ,  $K_{\omega i} = 125$  y  $K_{I_s} = 210$ . The simulation was carried out using a Runge-Kutta method with a fixed time step equal to  $0.0001s$ .

Speed tracking is shown in Fig. 3. Good performance of the controller is observed with a mean square error of  $0.8598$  rad/s. The speed curve  $\omega_{ss}$ , when the machine is modeled by a simplified  $dq0$  stationary model, is also shown in Fig. 3. It is worth noticing that the  $dq0$  model does not take into account the nonlinearity of the ferromagnetic material and a precise calculation of eddy-currents as in the case of the FE model.

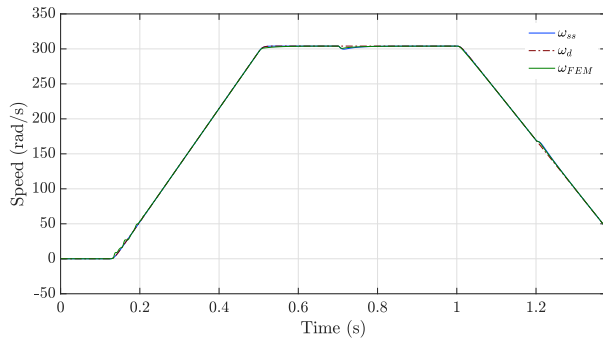


Fig. 3. Speed tracking.

Voltage and current signals are shown in Fig. 4 and Fig. 5, respectively. It can be seen that the control signals are adjusted both in magnitude and frequency to achieve the desired speed. Notice that in the time interval between  $0.7$  s and  $1$  s, corresponding to nominal operating condition, the supply voltages are up to  $40.2\%$  larger than the nominal peak value of  $537$  V. This is an unreachable operating condition in an experiment because it implies that the controller enters in a saturation regime. Meanwhile, the currents exceed the nominal peak value of  $12.57$  A by up to  $9.7\%$  in the same period of time. This is not a problem because the motors are designed to withstand an overload of  $1.25$  times their nominal current for a long period of time.

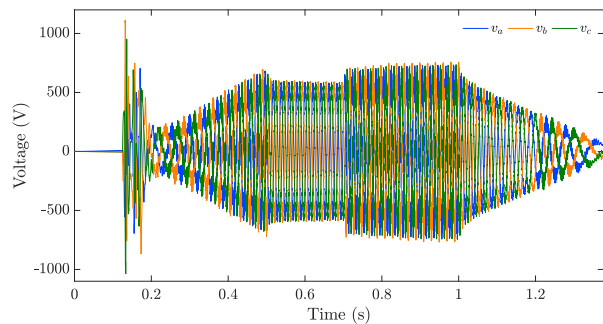


Fig. 4. Control signals with the motor modeled by FEM.

The voltage and current values at phase  $a$  of the motor are compared in Fig. 6 and Fig. 7, respectively. It can be seen that the problem of critical over-excitation does not arise using the state-space model because in the worst case the voltage

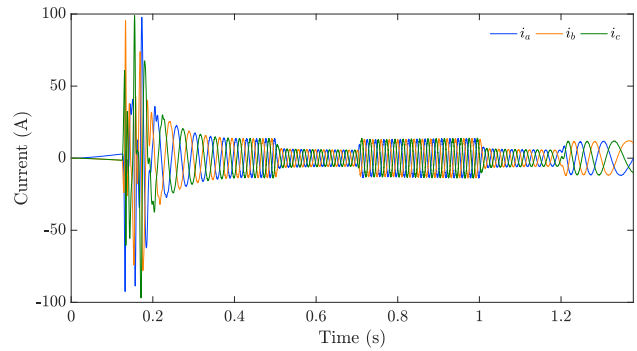


Fig. 5. Currents with the motor modeled by FEM.

exceeds by only  $7.6\%$  its nominal value. The difference in the voltage magnitude is attributed to the material nonlinearity considered in the cosimulation, in contrast with the linear representation used with the state-space model. Another factor is that speed is not a smooth signal when the machine is modeled with FE, just like in a real motor. Then, the controller tries to compensate for variations in speed, increasing the level of excitation to the motor in order to reach the desired speed at each instant of time. Voltage and speed signals could be filtered, but a lot of relevant information is lost and the advantage to use distributed models loses meaning.

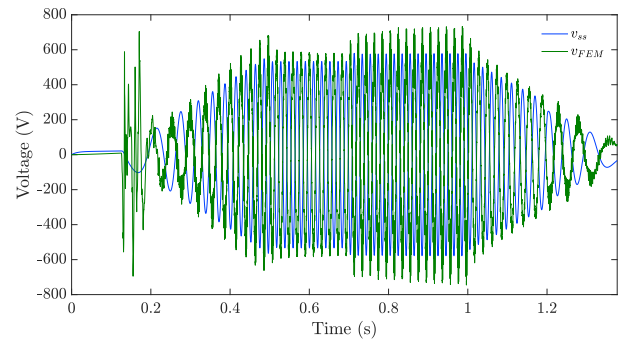


Fig. 6. Phase  $a$  voltage curves: FEM vs state-space model.

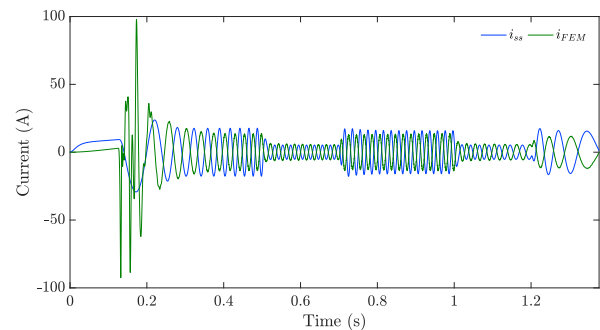


Fig. 7. Phase  $a$  current curves: FEM vs state-space model.

Regarding the computational cost, the simulation was performed on a computer with  $64$  GB of RAM, Intel Xeon Processor  $3.0$  GHz and  $16$  cores. The real-time needed to

complete the simulation was 39 hrs. It is well known that for a distributed model such a FE model the CPU time is much larger than for space-state models. However, some problems required to work with precise models to obtain reliable results as in the case of the problem addressed in this work.

## VI. CONCLUSIONS

The virtual test bench based on the cosimulation of finite element analysis and circuit simulation proves to be a powerful and reliable tool to evaluate control strategies for induction motors. The results show the importance of considering the entire electromagnetic phenomenon in the machine through a finite element model, when the motor operates above its nominal values.

It should be emphasized that significant differences were found in the results using the state-space model, which is commonly used as a starting point to evaluate controllers when compared with the finite-element model. This work highlights that for certain conditions the results are not reliable and it is recommended to resort to more sophisticated models before conducting experimental tests, to ensure personnel safety.

The analysis tool is not limited to the problem of induction motor control. The idea can be applied to analyze and solve problems in other types of machines with applications for example in hybrid vehicles, home appliances, and wind generation systems.

## ACKNOWLEDGMENT

This work was supported in part by CONACYT-MEXICO through project CB-2015/256519 and in part by the National System of Researchers (SNI-MEXICO).

## REFERENCES

- [1] A. Rihar, P. Zajec, and D. Voncina, "Cosimulation of ansys simplorer and matlab/simulink," in *2017 19th International Conference on Electrical Drives and Power Electronics (EDPE)*, Oct 2017, pp. 313–317.
- [2] P. Zhou, D. Lin, W. Fu, B. Ionescu, and Z. Cendes, "A general cosimulation approach for coupled field-circuit problems," *IEEE Trans. Magn.*, vol. 42, no. 4, pp. 1051–1054, 2006.
- [3] S. Schops, H. De Gerssem, and A. Bartel, "A cosimulation framework for multirate time integration of field/circuit coupled problems," *IEEE Trans. Magn.*, vol. 46, no. 8, pp. 3233–3236, Aug 2010.
- [4] S. Seman, J. Niiranen, and A. Arkkio, "Ride-through analysis of doubly fed induction wind-power generator under unsymmetrical network disturbance," *IEEE Trans. Power Systems*, vol. 21, no. 4, pp. 1782–1789, Nov 2006.
- [5] W. Zhao, M. Cheng, K. T. Chau, W. Hua, H. Jia, J. Ji, and W. Li, "Stator-flux-oriented fault-tolerant control of flux-switching permanent-magnet motors," *IEEE Trans. Magn.*, vol. 47, no. 10, pp. 4191–4194, Oct 2011.
- [6] X. Zhu, M. Cheng, W. Zhao, C. Liu, and K. Chau, "A transient cosimulation approach to performance analysis of hybrid excited doubly salient machine considering indirect field-circuit coupling," *IEEE Trans. Magn.*, vol. 43, no. 6, pp. 2558–2560, 2007.
- [7] A. K. Singh, P. Kumar, C. U. Reddy, and K. Prabhakar, "Simulation of direct torque control of induction motor using simulink, simplorer and maxwell software," in *2015 IEEE International Transportation Electrification Conference (ITEC)*, Aug 2015, pp. 1–6.
- [8] E. Bostanci, Z. Neuschl, and R. Plikat, "Influence of phase magnetic couplings on phase current characteristics of multiphase bldc machines with overlapping phase windings," *IEEE Trans. Magn.*, vol. 51, no. 9, pp. 1–13, Sep. 2015.
- [9] B. Zhang, W. Deng, L. Ruan, T. Wang, J. Quan, Q. Cao, Y. Teng, W. Wang, Y. Yuan, and L. Li, "Field-circuit cosimulation of 500-kv transformers in ac/dc hybrid power grid," *IEEE Trans. Applied Superconductivity*, vol. 26, no. 4, pp. 1–5, June 2016.
- [10] H. Shin and J. Park, "Anti-windup pid controller with integral state predictor for variable-speed motor drives," *IEEE Trans. Industrial Electronics*, vol. 59, no. 3, pp. 1509–1516, March 2012.
- [11] M. Masiala, B. Vafakhah, J. Salmon, and A. M. Knight, "Fuzzy self-tuning speed control of an indirect field-oriented control induction motor drive," *IEEE Trans. Industry Applications*, vol. 44, no. 6, pp. 1732–1740, Nov 2008.
- [12] H. Mujica-Ortega and G. Espinosa-Pérez, "Evaluación de diferenciadores numéricos para la obtención de velocidad y aceleración en control de motores eléctricos," *Congreso Nacional de Control Automático, CENIDET, México*, 2015.
- [13] H. Mujica and G. E. Pérez, "Control no lineal basado en pasividad de motores de inducción para alto desempeño dinámico," *Revista Iberoamericana de Automática e Informática industrial*, vol. 11, no. 1, pp. 32–43, 2014.
- [14] H. Sira-Ramírez, F. González-Montañez, J. A. Cortés-Romero, and A. Luviano-Juárez, "A robust linear field-oriented voltage control for the induction motor: Experimental results," *IEEE Trans. Industrial Electronics*, vol. 60, no. 8, pp. 3025–3033, Aug 2013.
- [15] G. Meunier, *The finite element method for electromagnetic modeling*. John Wiley & Sons, 2010.
- [16] J. P. A. Bastos and N. Sadowski, *Electromagnetic modeling by finite element methods*. Publication by Marcel Dekker, 2003.
- [17] E. Melgoza-Vazquez, R. Escarela-Perez, and J. L. Guardado, "Generalized primitive stamps for nonlinear circuit-field coupling in the transient case," *IEEE Trans. Magn.*, vol. 53, no. 5, pp. 1–9, 2017.
- [18] *Flux 12.2: User's Guide. CAD Package for Electromagnetic and Thermal Analysis using Finite Elements*. Altair Engineering, France, 2016.